IEEE Access
Multidisciplinary | Rapid Review | Open Access Journal

Received September 6, 2018, accepted October 6, 2018, date of publication October 10, 2018, date of current version November 8, 2018.

Digital Object Identifier 10.1109/ACCESS.2018.2875197

Semi-Active Vibration Control for in-Wheel Switched Reluctance Motor Driven Electric Vehicle With Dynamic Vibration Absorbing Structures: Concept and Validation

BIN XU, CHANGLE XIANG, YECHEN QIN, (Member, IEEE), PENG DING, AND MINGMING DONG

School of Mechanical Engineering, Beijing Institute of Technology, Beijing 100081, China

Corresponding author: Yechen Qin (qinyechenbit@gmail.com)

This work was supported in part by the Beijing Natural Science Foundation under Grant 3184058, in part by the National Natural Science Foundation of China under Grant 51505031, and in part by the China Postdoctoral Science Foundation under Grant BX201600017.

ABSTRACT This paper presents novel algorithms for vibration control of the in-wheel motor (IWM) driven electric vehicles to improve its ride comfort and reduce IWM vibration. A quarter vehicle model is first developed based on a dynamic vibration absorbing structure (DVAS) driven by a switched reluctance motor (SRM). This model considers the coupled longitudinal-vertical dynamics and the unknown road profile as well as the unbalanced electromagnetic force induced by the SRM are treated as the excitation. The dynamics and boundary models of two commercially available semi-active dampers are then presented, which are used as the actuators of both the suspension and the DVAS structure. Based on the developed model, a hybrid controller with a hybrid acceleration driven damping algorithms is proposed to reduce the vibration of the sprung mass and the SRM. The controller parameters are subsequently determined by solving the multi-objective optimization problem with a multi-objective evolutionary optimization method. Numerical simulation results for random road and bumpy excitations are analyzed, and multi-body simulation is finally performed to validate the feasibility of the proposed controllers. Results indicate that the proposed hybrid controllers can effectively improve ride comfort and reduce the SRM vibration compared with the traditional suspension system with IWM.

INDEX TERMS Hybrid suspension control, in-wheel motor, switched reluctance motor, dynamic vibration absorbing structure, multi-body simulation.

I. INTRODUCTION

More strict vehicle emission standards and ful requirements for the traditional vehicle have paved the way to the development of electric vehicles (EVs) [1], [2], and dynamics control for EVs attracts much attention from both the automobile industry and academia in recent years [3]–[7]. EVs replace internal combustion engine with one or more motors, and it can be categorized into two main groups, namely, centrally driven and in-wheel motor (IWM) driven from the perspective of propulsion system [8]. Compared to the centrally driven, the IWM driven type introduces several advantages, including space and weight saving, fast system response, high energy efficiency, and flexible configuration [9]. Nevertheless, the performance of motors installed inside the wheels are severely constrained by the limited wheel hub space, and the increased unsprung mass will not only deteriorate ride comfort and road handling, but also reduce the lifespan of the motors due to the harsh vibration environment [10].

Contrasted with the suspension system of traditional vehicles, the suspensions of IWM driven EVs evolve into the coupled IWM-suspension system by integrating the functions of both vibration reduction and vehicle driving, and the unbalanced electromagnetic force (UEMF) caused by the air gap variation becomes an extra internal vibration source for the IWM-suspension system [11]. The IWM-suspension mutual effects between the IWM and the suspension thus

deserve further investigation. To date, various methods have been proposed to reduce IWM induced vibration and improve the dynamic performances of the IWM driven EVs. From the perspective of IWM control, Takiguchi *et al.* [12] used a current control algorithm to reduce the amplitude of the radial force. Sun *et al.* [13] improved suspension vertical responses during the IWM starting process with a modified current chopping controller. As for the suspension subsystem, the concept of dynamic vibration absorbing structure (DVAS) was proposed to improve IWM-suspension vertical responses. Hredzak *et al.* [14] and Nagaya *et al.* [15] connected the stator to either sprung mass or unpsprung mass with the DVAS, and numerical simulation results showed that such novel structure could improve vehicle ride comfort and road handling. Nevertheless, these research did not consider IWM and longitudinal dynamics. Qin *et al.* [11] presented a comparative study for different types of DVAS with the previously neglected motor dynamics and showed that by placing the DVAS between the stator and the unsprung mass, the system could achieve better performance. As noted by the papers above, the application of the DVAS introduces extra spring-damper components and forms a novel multi-inputs suspension system from the perspective of system control, which brings new challenges for vibration reduction of IWM driven EVs. By now, however, literature related to DVAS based IWM-suspension mainly focus on the suspension parameters optimization, and further improvement of the novel system is highly desired.

The controllable suspension system, which can be categorized into active and semi-active control, is considered as one of the most effective ways to improve vertical dynamics of the suspension system, and many remarkable works had been done in this field during the past two decades [16]–[21]. In recent years, active suspension system has been theoretically studied for IWM-suspension system. Shao *et al.* [22] and Wang *et al.* [23] synthesized active control force with H∞ theory, and simulation results showed considerable performance improvement. As the object used in these research was the traditional suspension model with only increased unsprung mass, the generated controller required to be improved for the real IWM-suspension system, which contains UEMF and longitudinal dynamics.

To solve the problems above and improve dynamic performances of IWM driven EVs, this paper presents two semi-active control algorithms for the novel DVAS based IWM-suspension system. Considering the dimension limits of the DVAS, two commercially available semi-active dampers are adopted as the actuators, and the contributions of this study can be concluded as follows:

- A DVAS based IWM-suspension system model with the motor and coupled vertical-longitudinal dynamics is developed, and semi-active control strategies are proposed to improve model vertical dynamic performance.
- The semi-active control force is allocated and realized by two commercially available controllable dampers located between the suspension and the DVAS, and a novel acceleration driven damping control strategy is proposed to reduce the required sensor number.
- The feasibility of the proposed model and semi-active suspension control algorithms is studied and validated by a multi-body simulation (MBS) software.

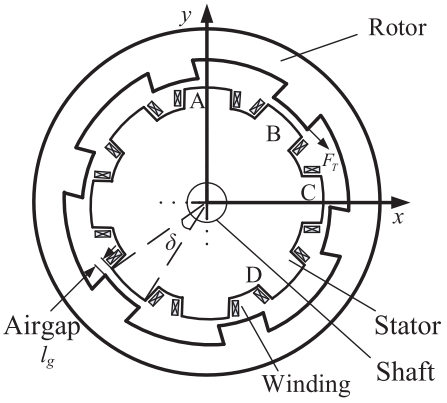

FIGURE 1. Scheme of the 8/6-four phasess SRM.

The rest of this paper is organized as follows: firstly, the SRM model is presented in Section 2. The DVAS based IWM-suspension system model, longitudinal dynamics, and controllable damper models are then introduced in Section 3. The proposed hybrid suspension controllers are illustrated in Section 4. Numerical simulations and MBS validations are carried out in Section 5. Conclusion and future work are discussed at last.

II. SRM MODELING

Commonly used IWMs include permanent magnet synchronous motor (PMSM) [24] and switched reluctance motor (SRM) [25]. PMSM has many advantages and is widely used in EVs. However, SRM is viewed as a strong candidate for IWM driven EVs shortly because of its merits, e.g., the dispensation of permanent magnets, firm and straightforward structure, and fault tolerance [10].

This section presents a Fourier series based nonlinear SRM model, and formalizes the output torque and the UEMF of the SRM.

A. ELECTROMAGNETIC AND VOLTAGE EQUATIONS

An 8/6-four phases SRM with an exterior rotor is adopted as the object in this paper, and its rated power is 5kW. The schematic of the SRM is shown in Fig. 1. The rotor is fully aligned to the stator pole when the rotor position $\theta = 30°$, and $\theta = 0°$ corresponds to the fully unaligned position.

The magnetic co-energy is defined as:

$$W(i,\theta) = \int_0^i \psi(\theta, i)\, di \tag{1}$$

where i is the phase current and $\psi(\theta, i)$ is the flux linkage. Considering that both i and inductance $L(\theta, i)$ determine $\psi(\theta, i)$, this paper uses Fourier series based method to express $L(\theta, i)$.

By considering the first three terms of the Fourier expansion, the inductance $L(\theta, i)$ can be written as [26]:

$$L(\theta, i) = L_0(i) + L_1(i)\cos(N_r\theta + \pi) + L_1(i)\cos(2N_r\theta + 2\pi) \quad (2)$$

where L_0, L_1, and L_2 are functions of the current i, which can be calculated according to:

$$\begin{cases} L_0(i) = [(L_a(i) + L_u)/2 + L_m(i)]/2 \\ L_1(i) = (L_a(i) - L_u)/2 \\ L_2(i) = [(L_a(i) + L_u)/2 - L_m(i)]/2 \end{cases} \quad (3)$$

where L_a, L_u, and L_m are the inductance of the aligned position, the unaligned position, and mid-way position, respectively. $L_a(i)$ and $L_m(i)$ can be fitted by two coefficients:

$$L_a(i) = \sum_{n=0}^{3} a_n i^n, \quad L_m(i) = \sum_{n=0}^{3} b_n i^n \quad (4)$$

According to Faraday-Lenz Law, the flux linkage can be expressed as $\psi(\theta, i_k) = \int_0^{i_k} L(i_k, \theta)\, di_k$. Then by defining $c_n = a_{n-1}/n$ and $d_n = b_{n-1}/n$ ($c_0 = d_0 = 0$), the flux linkage of any phase k can be calculated as:

$$\psi(\theta, i_k) = \frac{1}{2}\left[\cos^2(N_r\theta) - \cos(N_r\theta)\right] \times \sum_{n=0}^{3} c_n i^n + \frac{1}{2}L_u i_k\left[\cos^2(N_r\theta) + \cos(N_r\theta)\right] + \sin^2(N_r\theta)\sum_{n=0}^{N} d_n i^n \quad (5)$$

With the flux linkage given in (5), the voltage of phase k can be expressed as follows [27]:

$$U_k = R_k i_k + \frac{d\psi_k}{dt} = R_k i_k + L_k(\theta, i_k)\frac{di_k}{dt} + w\frac{\partial\psi_k}{\partial\theta} \quad (6)$$

where w is the angular velocity of the rotor. The phase current i_k can be formulated based on (6):

$$i_k = \int \frac{U_k - R_k i_k - w\frac{\partial\psi_k}{\partial\theta}}{L_k(\theta, i_k)} dt \quad (7)$$

B. ELECTROMAGNETIC TORQUE AND UEMF

Since the co-energy equals to the mechanical energy, the torque T and the radial force F_r of a SRM can be calculated based on the co-energy defined in (1):

$$T = \left.\frac{\partial W(\theta, i)}{\partial\theta}\right|_{i=const}, \quad F_r = \left.\frac{\partial W(\theta, i)}{\partial l_g}\right|_{i=const} \quad (8)$$

where l_g is the air gap between the stator and the rotor as shown in Fig. 1.

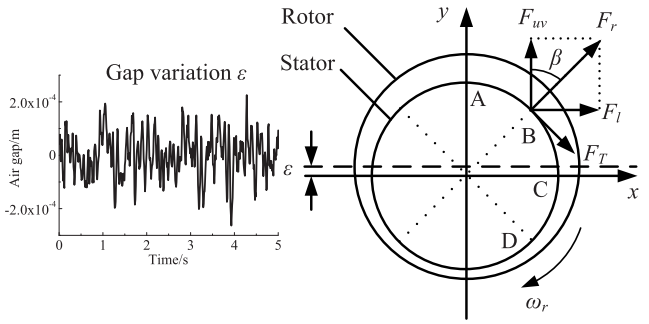

FIGURE 2. Unbalanced radial force induced by air gap eccentricity.

The phase k torque of the SRM can be formulated by combining (8) and (5), as follows:

$$T_k = \int_0^{i_k} \frac{\partial\psi(\theta, i_k)}{\partial\theta} di_k = \sin(N_r\theta)\sum_{n=1}^{3}\frac{1}{n}e_{n-1}i_k^n + \sin(2N_r\theta)\sum_{n=1}^{3}\frac{1}{n}f_{n-1}i_k^n \quad (9)$$

where e_n and f_n are defined as:

$$\begin{cases} e_0 = 0, e_1 = (1/2)N_r(c_1 - L_u), \\ f_0 = 0, f_1 = (1/2)N_r(2d_1 - c_1 - L_u) \\ e_n = (1/2)N_r c_n, f_n = N_r d_n - e_n \end{cases} \quad (10)$$

Then, the total torque is defined as $T_{overall} = \sum_{k=1}^{4} T_k$.

Similar to the torque, the phase k radial force can be calculated as [27]:

$$F_{rk} = -\frac{T_k\delta}{l_g} \quad (11)$$

where δ is the overlap angle between the stator and the rotor of the investigated phase k. Note that the radial force is inversely proportional to the air gap l_g, which means the air gap variation between the opposite stator poles will result in the UEMF and affect vehicle system responses. Considering the air gap eccentricity ε, the SRM radial force is depicted in Fig. 2, and the overall vertical UEMF can be expressed as [11]:

$$F_{uv} = \sum_{k=1}^{4}\left\{\left[-\frac{T_k\delta}{l_g - \varepsilon\sin\beta_k} + \frac{1}{2}\frac{T_k\delta}{l_g + \varepsilon\sin\beta_k}\right]\cos\beta_k\right\} \quad (12)$$

where β_k is the angle between the stator phase k and the vertical axle, and $\beta_1 = 0°$, $\beta_2 = 45°$, $\beta_3 = 90°$, and $\beta_4 = 135°$. Previous research indicated that the presence of the UEMF will mainly influence the vibration of the unsprung mass [11].

III. SUSPENSION MODELING

This section successively introduces the DVAS based suspension system, longitudinal dynamics, and controllable damper models.

A. DVAS BASED SUSPENSION SYSTEM

The structures and the superiorities of the DVAS based suspension system has been well studied in [11]. According to the results, this paper uses a tire type DVAS based suspension as the object and its configuration is depicted in Fig. 3.

The dynamics of both passive and DVAS based suspension systems can be described by Newton's motion law, as following:

$$\begin{aligned} m_b\ddot{x}_b + k_s\left(x_b - x_{sa}\right) + c_s\left(\dot{x}_b - \dot{x}_{sa}\right) &= 0 \\ m_{sa}\ddot{x}_{sa} + k_s\left(x_{sa} - x_b\right) + c_s\left(\dot{x}_{sa} - \dot{x}_b\right) & \\ + k_{sa}\left(x_{sa} - x_{wa}\right) + F_d &= 0 \\ m_{wa}\ddot{x}_{wa} + k_t\left(x_{wa} - x_z\right) + k_{sa}\left(x_{wa} - x_{sa}\right) - F_d &= 0 \end{aligned} \tag{13}$$

$$\begin{aligned} m_b\ddot{x}_b + k_s\left(x_b - x_{s1}\right) + c_s\left(\dot{x}_b - \dot{x}_{s1}\right) &= 0 \\ m_r\ddot{x}_r + k_b\left(x_r - x_s\right) + F_d &= 0 \\ m_s\ddot{x}_s + k_d\left(x_s - x_{s1}\right) + k_b\left(x_s - x_r\right) & \\ + c_d\left(\dot{x}_s - \dot{x}_{s1}\right) - F_d &= 0 \\ m_{s1}\ddot{x}_{s1} + k_t\left(x_{s1} - x_z\right) + k_s\left(x_{s1} - x_b\right) & \\ + c_s\left(\dot{x}_{s1} - \dot{x}_b\right) + k_d\left(x_{s1} - x_s\right) & \\ + c_d\left(\dot{x}_{s1} - \dot{x}_s\right) &= 0 \end{aligned} \tag{14}$$

where x_* represents displacement, and the subscripts b, sa, wa in Fig. 3(a) refer to the sprung mass, the total mass of the stator and the axle, and the rotor mass, respectively. As for the DVAS based IWM-suspension system, the subscripts $s1$, r, s stand for the total mass of the unsprung component and axle, the rotor mass, and the stator mass, respectively. x_z is road unevenness. In Fig. 3, $F_d = F_{uv}$ is the vertical UEMF, and the values of all other parameters in (13) and (14) will be discussed later.

The DVAS in Fig. 3(b) connecting the axle and the stator, is composed of a spring and a damper. The connection indicates that the DVAS can vertically support the stator and reduce the vibration caused by road unevenness. The physical realization will be discussed in the next step.

This paper will then synthesizes two time-varying controllable damper force to replace the passive force appearing in both the suspension and the DVAS, i.e., $c_s\left(\dot{x}_b - \dot{x}_{s1}\right)$ and $c_d\left(\dot{x}_{s1} - \dot{x}_s\right)$.

B. LONGITUDINAL DYNAMICS

The torque generated by the SRM will drive the vehicle forward and backward. The rotational dynamics of the driving wheel is given below [28], [29]:

$$J\dot{\omega}_r = T_{wheel} - rF_x \tag{15}$$

where J is the wheel inertia; $\omega_r = w$ is the wheel angular velocity; $T_{wheel} = T_{overall}$ is the overall torque generated by the SRM; r is the tire effective rolling radius, and F_x is the longitudinal force generated by the friction between the tire and ground. In this paper, the Magic Formula is used as the nonlinear tire longitudinal model, and the parameters of the model are derived from a Michelin MXV8 205/55R16 tire [30], [31].

With the longitudinal tire force F_x, the vehicle longitudinal dynamics equation can be expressed as:

$$M\dot{v} = F_x - R_x - F_{air} \tag{16}$$

where M is the total mass; v represents velocity velocity. F_{air} corresponds to the aerodynamic drag force, and R_x stands for the rolling resistance. Both F_{air} and R_x can be calculated as:

$$F_{air} = \frac{C_D A v^2}{21.15}, \quad R_x = \mu F_n \tag{17}$$

where C_D, A, and μ represent the drag coefficient, vehicle frontal area, and rolling resistance coefficient, respectively. F_n is the vertical load, which can be expressed as [32]:

$$F_n = \left(m_b + m_w\right) g - k_t\left(x_w - x_z\right) \tag{18}$$

Generally, the road unevenness results in the airgap variation, which induces the UEMF and deteriorates IWM-suspension system vertical responses. Meanwhile, the torque generated by the SRM balance the forces caused by air motion and road friction in the longitudinal direction. More details on the vertical-longitudinal coupled dynamics, refer to [11].

C. CONTROLLABLE DAMPER MODEL

Different kinds of controllable dampers have been developed to mitigate system vibration, and they have been commercialized in numerous mid-to-high end vehicles, including Cadillac Seville STS, Acura MDX, and GM-Lacrosse, etc. [33], [34]. Among all damper categories, both magneto-rheological (MR) and proportional valve are the most frequently used types in the automobile industry [33]. This paper uses these two types of controllable dampers to improve system performance. A continuous damping control (CDC) damper from ZF Sachs is used to generate the suspension controllable damper force [33], and a smaller MR damper from Lord is utilized in the DVAS due to the limited space. The suspension damper force F_{cs} and DVAS damper force F_{cd} can be formulated as:

$$\begin{aligned} F_{cs} &= f_1\left(i_{cs}, \dot{x}_b - \dot{x}_{s1}\right) \\ F_{cd} &= f_2\left(i_{cd}, \dot{x}_{s1} - \dot{x}_s\right) \end{aligned} \tag{19}$$

Many methods like Bouc-Wen and polynomial models can be used [35]–[37] to accurately depict such functions, and this paper adopts a nonparametric model [38], in which the controllable damper force is expressed as:

$$\begin{aligned} F_{damper} &= A\left(i_{damper}\right) \cdot S_b\left(v_{relative}\right), \\ A\left(i_{damper}\right) &= \sum\nolimits_{n=0}^{k} a_n i_{damper}^n, \\ S_b\left(v_{relative}\right) &= \tanh\left[\left(b_1 i_{damper} + b_0\right) v_{relative}\right] \end{aligned} \tag{20}$$

where n is the function order, and this paper uses $n = 2$. a_n and b_n are coefficients to be determined, and i is the control current. This paper applies particle swarm optimization (PSO) to estimate all the unknown coefficients in (20), based on which the control current can be expressed as

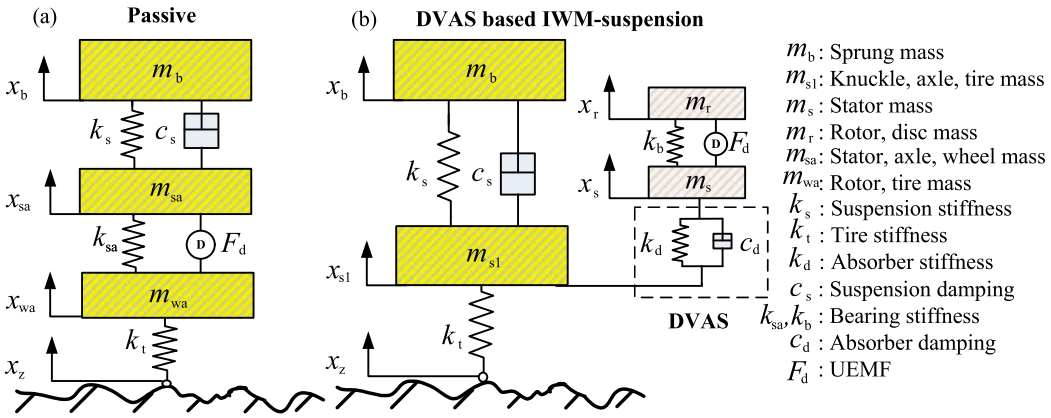

FIGURE 3. IWM driven EVs suspension model: (a) Passive, (b) DVAS based IWM-suspension.

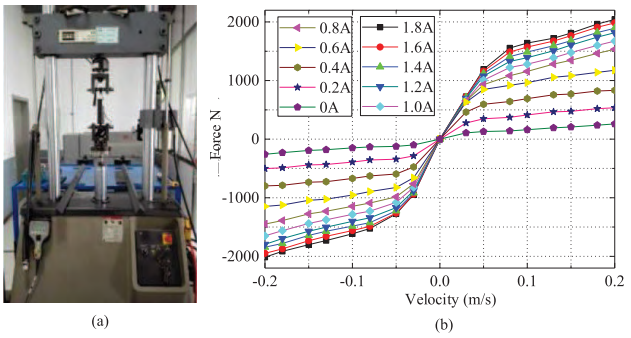

FIGURE 4. MR damper manufactured by Lord: (a) damper in the test rig, (b) force-velocity map.

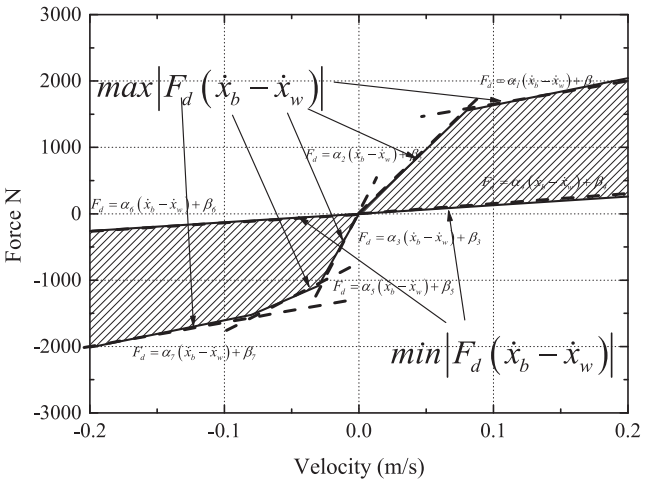

FIGURE 5. MR damper boundary model.

$i = f^{-1}\left(F_{damper}, v_{relative}\right)$ and calculated. For more details, refer to [33]. The two adopted controllable dampers are modeled based on the above equations, and the load frame with the mounted MR damper is shown in Fig. 4(a) along with the velocity-force map depicted in Fig. 4(b).

Note that the damper dynamics depicted in (20) do not constrain the output force. The calculated force may be unrealizable and thus results in excessive or negative control current. A damper boundary model derived from Fig. 4(b) is also applied in this paper [33], as shown in Fig. 5. The relationship between the boundary model and the damper model in (20) will be illustrated in the next section.

IV. DVAS BASED SUSPENSION HYBRID CONTROL

To evaluate controller performance, this section first treats suspension control as a multi-objective optimization problem (MOOP), and then develops a hybrid controller for the multi-inputs DVAS based suspension system. A novel hybrid acceleration driven damping (hybrid-ADD) algorithm is then proposed to reduce the total sensor number. This section finally uses a multi-objective evolutionary based optimization method to compute the controller parameters.

A. MOOP FORMULATION

The purpose of suspension design is to find the balance point among multiple objectives, and previous research always treated suspension system control as a MOOP under the constraint of rattle space [16], [39], [40]. For the IWM-suspension system, the induced vibration from the SRM will not only deteriorate the suspension system performance but also result in premature fatigue failure and damage components like bearings and gears [41]. To improve ride comfort and reduce motor vibration for the novel IWM-suspension system, the MOOP to be solved is defined as (21).

$$\begin{aligned} &min \quad g_1(P) = \sigma_{\ddot{x}_b}, \quad g_2(P) = \sigma_{\ddot{x}_s}, \\ &subject\ to \quad RS \le \lim(RS), \\ &\qquad air \le \lim(air), \quad TD \le \lim(TD) \end{aligned} \tag{21}$$

where $P \in \Re$ is the controller parameters to be designed. $\sigma_{\ddot{x}_b}$ is the root mean square (RMS) of the sprung mass acceleration (SMA), which represents the ride comfort. $\sigma_{\ddot{x}_s}$ stands for the RMS of the stator acceleration (SA), corresponding to the vibration condition of the SRM. RS, air, and TD are

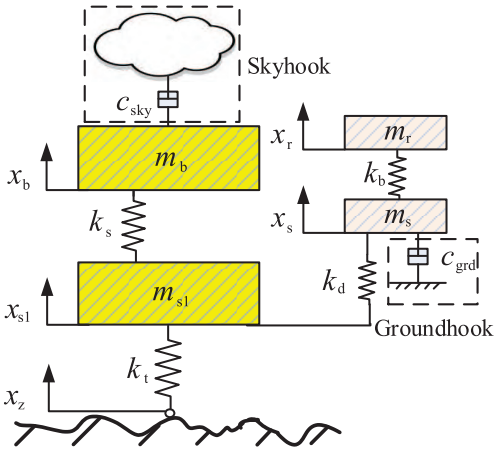

FIGURE 6. structure of the novel hybrid controller for the DVAS based IWM-suspension system.

the rattle space $x_b - x_{s1}$, air gap between stator and rotor $x_s - x_r$, and tire deflection $x_{s1} - x_z$ for the DVAS based structure shown in Fig. 3 (b), respectively. Note that both constraints of *RS* and *air* are used to prevent the masses from hitting the limits, and lim (*TD*) is used to ensure the tire keep contacting the ground, which is viewed as the criterion of the road handling ability. The three constraints are defined as $\lim(RS) = 0.1\text{m}$, $\lim(air) = 0.001\text{m}$, and $\lim(TD) = 0.018\text{m}$ [11]. Based on the MOOP, the goal of the controllers can be concluded as to balance the performance of the ride comfort and stator acceleration by maintaining *RS*, *air*, and *TD* within the constraints.

B. HYBRID CONTROL ALGORITHM

As the most classical semi-active control algorithm, skyhook control was proposed to reduce vehicle chassis vertical vibration by virtually linking the vehicle sprung mass to the sky [42]. Groundhook control performed in the dual way to the skyhook algorithm to improve road handling ability [43]. By combining the advantages of these algorithms, a hybrid control was then presented, which was realized by a single controllable damper placed between the sprung mass and the unsprung mass [39]. Similar to the traditional hybrid control, the ideal structure of the novel hybrid controller for the formulated DVAS based model (14) is proposed to reduce the sprung mass acceleration and the stator acceleration (21), as shown in Fig. 6.

It can be seen from Fig. 6 that the ideal structure requires two virtual dampers with coefficients of c_{sky} and c_{grd} connecting to the sky and the ground, respectively. Since the framework described above is theoretically impossible, this paper uses the control laws of both skyhook and groundhook control to mimic the behaviour of the virtual damper. Different from the traditional suspension system, the extra controllable damper located inside the DVAS makes the imitation by two controllable dampers possible, and the force conflict issue appeared in the traditional hybrid algorithm is solved by the proposed method. The control laws of the novel hybrid suspension control can be expressed as:

$$c_{cs} = \begin{cases} c_{sky}, & if\ \dot{x}_b\,(\dot{x}_b - \dot{x}_{s1}) \geq 0, \\ c_{\min}, & if\ \dot{x}_b\,(\dot{x}_b - \dot{x}_{s1}) < 0 \end{cases} \tag{22}$$

$$c_{cd} = \begin{cases} c_{grd}, & if\ \dot{x}_s\,(\dot{x}_s - \dot{x}_{s1}) \geq 0, \\ c_{\min}, & if\ \dot{x}_s\,(\dot{x}_s - \dot{x}_{s1}) < 0 \end{cases} \tag{23}$$

where c_{cs} and c_{cd} are skyhook and groundhook control coefficients, which will be selected in the following section to replace the passive dampers, i.e., c_s and c_d in Fig. 3(b).

C. HYBRID-ADD CONTROL ALGORITHM FOR IWM-SUSPENSION SYSTEM

The novel IWM-suspension system defined by (14) suspends the SRM with the dynamic absorbing structure, based on which the proposed hybrid controller (22), (23) requires more responses to be measurable compared to the traditional hybrid control. It can be seen that the proposed controller needs the velocities of the sprung mass x_b, the rattle space $x_b - x_w$, the stator x_s, and the DVAS displacement $x_s - x_{s1}$. Since these velocities cannot be directly measured, one way is to place two accelerometers on the sprung mass and the stator, and use two LVDTs to measure the rattle space and the displacement of the DVAS. The four required velocities can then be derived by integrating the accelerations and calculating the derivate of the displacement. Considering the inner space limitation of the DVAS and the requirement of multiple sensors (totally 16 sensors are required for a full vehicle driven by four IWMs), this paper further presents a more straightforward algorithm, named hybrid acceleration driven damping (ADD) control, to reduce the system vibration. ADD was first proposed by Savaresi *et al.* [44] and can provide better performance beyond the sprung mass resonance frequency. The hybrid-ADD control law can be described by (24).

$$\begin{aligned} c_{csADD} &= \begin{cases} c_{\min-ADD}, & if\ \ddot{x}_b^2 - \alpha^2\dot{x}_b^2 \geq 0 \\ c_{sky-ADD}, & if\ \ddot{x}_b^2 - \alpha^2\dot{x}_b^2 < 0 \end{cases} \\ c_{cdADD} &= \begin{cases} c_{\min-ADD}, & if\ \ddot{x}_s^2 - \alpha^2\dot{x}_s^2 \geq 0 \\ c_{grd-ADD}, & if\ \ddot{x}_s^2 - \alpha^2\dot{x}_s^2 < 0 \end{cases} \end{aligned} \tag{24}$$

where $c_{min-ADD}$, $c_{sky-ADD}$, $c_{grd-ADD}$, and α are positive constants to be designed. It can be seen from (24) that the hybrid-ADD is very simple, which uses only $\ddot{x}_b$, $\dot{x}_b$, $\ddot{x}_s$, and $\dot{x}_s$. Since the velocities can be obtained by numerical integration of the corresponding acceleration signal, only two accelerometers mounted on the sprung mass and the stator are required, and a total of 8 accelerometers is needed for a full vehicle driven by four IWMs.

D. CONTROLLER PARAMETERS OPTIMIZATION

Previous research showed that the parameters play an important role in the semi-active control strategies [33], and an analytical expression based controller parameter selection method performed well for the linear suspension

system [39], [45]. As for the nonlinear suspension system, the inherent nonlinearities, time delay, and uncertainties make the above method impractical. The evolutionary algorithms (EA) are thus proposed to overcome the above limitation. Since most EAs are based on Monte-Carlo method, this paper uses a recently published method, named multi-objective evolutionary algorithm based on decomposition (MOEA/D) [46], to solve the MOOP given in (21). MOEA/D decomposes a MOOP into several multiple sub-optimization issues, and can produce the optimized results with a uniform distribution by a small population size. Therefore, the computational complexity of MOEA/D is much smaller than other EAs.

MOEA/D uses the scalar aggregate functions (SAF) to define the neighborhood relations of the optimization sub-problems, which are evaluated based on the relative distance. One advantage of MOEA/D is that the optimal solution of any two adjacent sub-problems are similar, and each sub-problem only uses the adjacent information. Considering the objective functions and the constraints given in (21), the flow chart of the MOEA/D is shown in Table (1).

The concept of penalty function is used in this paper to deal with the constraints shown in (21) [47]. For a solution x to the MOOP that meets the constraints, its constraint violation degree is defined as [48]:

$$Z(x) = \left| \sum_{j=1}^{p} \min\left(g_j(x), 0\right) \right| \tag{25}$$

where $g_j(\cdot)$ is the j^{th} constraints. For the P_r defined in Step 5, we set:

$$Z_{\min} = \min\left\{ Z\left(x^i\right), i \in P_r \right\},$$
$$Z_{\max} = \max\left\{ Z\left(x^i\right), i \in P_r \right\}.$$

The threshold value τ is defined as:

$$\tau = Z_{\min} + 0.3\left(Z_{\max} - Z_{\min}\right) \tag{26}$$

The $g^{te}(\cdot)$ in Step 8 is then defined as:

$$g^{te}(x|\lambda, z) = \begin{cases} g^{te}(x|\lambda, z) + s_1 Z^2(x), & if\ Z(x) < \tau \\ g^{te}(x|\lambda, z) + s_1\tau^2 + s_2\left(Z(x) - \tau\right), & else \end{cases} \tag{27}$$

It can be observed from (25)-(27) that the penalty function can automatically search the feasible region, and the function value will increase sharply when $Z(x)$ exceeds the threshold τ, which ensures the system responses will not violate the constraints defined in (21).

V. NUMERICAL SIMULATION

This section first introduces the simulation settings, and then compares the numerical simulation results for different IWM-suspension structures under random and bumpy road excitations. A multi-body software (MBS) validation is presented at last to illustrate the feasibility of the proposed controllers.

TABLE 1. Algorithm: MOEA/D.

Input
· MOOP
· The stopping criterion
· The total number N of the sub-problems in the MOEA/D;
· The neighborhood number V of each weight vector.
Output
· Optimized parameters set P
Step 1
· Parameter initialization and set $P = \emptyset$;
Step 2
· Compute the distances between any two weight vectors and then calculate the V closest weight vectors to each other. For each sub-problem $i = 1, \ldots, N$, set $A(i) = \{i_1, \ldots, i_V\}$, where $\lambda^{i_1}, \ldots, \lambda^{i_V}$ are the V closest weight vectors to λ^i;
Step 3
· Randomly generate an initial population $x^1, \ldots x^N$, and set $F^i = F\left(x^i\right)$;
Step 4
· Generate and initialize $z = (z_1, \ldots, z_m)$ by a problem-specific method [46];
Step 5
· Uniformly randomly generate a number $rand$ from (0,1), then set [47]:

$$P_r = \begin{cases} A(i), & rand < 0.9 \\ \{1, \ldots, N,\}, & else \end{cases}$$

Randomly select $P_r(l)$ and $P_r(k)$ from $P_r(i)$, and then generate a solution y from x_l and x_k by using genetic operators;
Step 6
· Apply an approach to heuristically repair/improve y, and output y', if an element of y' falls out of the constraints, then its value is reset to be a random value inside the constraints;
Step 7
· For each $j = 1, \ldots, m$, if $z_j < f_j(y')$, then set $z_j = f_j(y')$;
Step 8
· for each index $j \in P_r(i)$, if $g^{te}\left(y'|\lambda^j, z\right) \leq g^{te}\left(x^j|\lambda^j, z\right)$, then set $x^j = y'$ and $F^j = F(y')$, where $g^{te}(\cdot)$ is the objective function of any sub-problem;
Step 9
· Remove all vectors in P that are dominated by $F(y')$, else add $F(y')$ to P;
Step 10
· If stopping criteria is satisfied, then stop and output P, else go to **Step 2**.

A. SIMULATION SETTINGS

Based on the created damper model and the developed controllers, the overall control structure can be depicted in Fig. 7. This structure includes three parts, namely semi-active

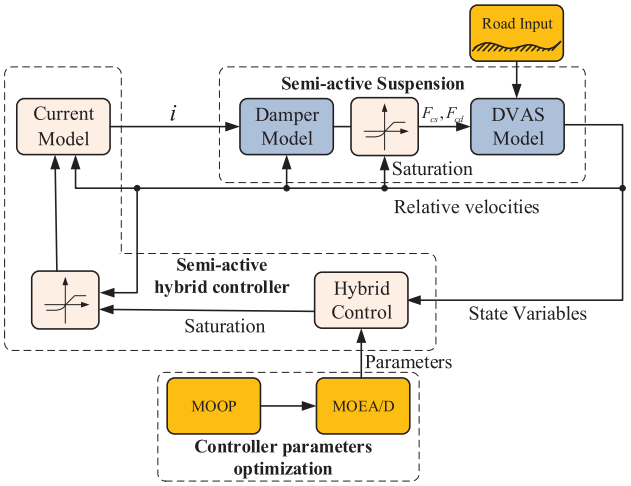

FIGURE 7. Hybrid control scheme for DVAS based IWM-suspension system.

TABLE 2. SRM-suspension system parameters.

Parameters	Value	Parameters	Value
m_b	332 kg	m_s	20 kg
m_{sa}	70 kg	m_{s1}	25 kg
k_s	15800 N/m	m_r	25 kg
c_s	1270 Ns/m	k_d	53000 N/m
k_t	220000 Ns/m	c_d	1900 Ns/m
k_b	1.4×10^7 N/m	C_D	0.28
A	1.6 m^2	μ	0.0066
J	0.9 kgm^2	r	0.316 m

suspension, semi-active hybrid controller, and parameters optimization. Note that the optimization part generates the optimized controller parameters off-line and prestores them in the ECU for further application. In the semi-active hybrid controller part, the stored parameters and the states obtained from the plant are taken as the controller input, and the controller generates control force F. Then, both the boundary and the current model output realizable control force and current i. The damper model given in (20) finally synthesize the control force to improve the IWM-suspension system dynamics responses.

In this paper, the weights of $g_1(P)$ and $g_2(P)$ are set to be identical, which means the ride comfort and the vibration of SRM have the same importance. This assumption provides a fair comparison of the different structures and controllers. The fixed system parameters are shown in Table 2 [11].

The controller parameters are then optimized based on the above assumption, and Table 3 shows the optimized values. With the ranges shown in the third column, MOEA/D generates the optimized values as shown in the fourth column. It can be seen that all of the optimized values satisfy the constraints.

The numerical simulation results are carried out under two different road excitations. For the random road excitation, the vehicle is traveling at 60 km/h on ISO road level B.

TABLE 3. SRM-suspension system parameters.

Parameters	Range	Value
c_s (DVAS)	600-5000 Ns/m	1160 Ns/m
c_d (DVAS)	600-5000 Ns/m	1870 Ns/m
c_{sky}	600-4000 Ns/m	2840 Ns/m
c_{grd}	600-4000 Ns/m	1120 Ns/m
c_{min}	100-1000 Ns/m	210 Ns/m
$c_{sky-ADD}$	600-4000 Ns/m	2480 Ns/m
$c_{grd-ADD}$	600-4000 Ns/m	960 Ns/m
$c_{min-ADD}$	100-1000 Ns/m	180 Ns/m

TABLE 4. RMS comparison for random road excitation.

RMS	Passive	DVAS	Hybrid	Hybrid-ADD
SMA (m/s^2)	0.8053	0.5535	0.5092	0.5049
SA (m/s^2)	9.09	3.46	3.37	3.46
RS (m)	0.0041	0.0061	0.0072	0.0078
Airgap (m)(1e-5)	-	0.627	0.599	0.624
TD (m)	0.0021	0.0017	0.0016	0.0016

In terms of the generation of random road profile, readers can refer to [49]–[51]. The bump input is defined according to [52], where v is the vehicle velocity:

$$x_z = \begin{cases} 0.025\,[1+\sin(2\pi vt/2.5)], & 1 < t < 1+2.5/v \\ 0 & otherwise \end{cases} \quad (28)$$

For the sake of the simplicity, all the four IWM-suspension structures are named as:

1) Passive: the conventional IWM-suspension system described by (13);
2) DVAS: the DVAS based IWM-suspension system described by (14);
3) Hybrid: DVAS based IWM-suspension system with controller defined by (22), (23);
4) Hybrid-ADD: DVAS based IWM-suspension system with controller defined by (24).

B. SIMULATION RESULTS UNDER DIFFERENT ROAD EXCITATIONS

Simulation results for random road excitation are tabulated in Table 4, and PSD comparison is depicted in Fig. 8.

According to Table 4, it can be observed that all three suspension systems with the DVAS can improve both ride comfort and reduce motor vibration. Application of the DVAS structure can reduce 31.3% of SMA, and 61.9% of SA compared to the passive structure. For the two types of controllers, the hybrid controller can further achieve 8% improvement in SMA, and 2.6% improvement of SA w.r.t. the DVAS. As for the hybrid-ADD, 8.8% improvement in SMA w.r.t. the DVAS can be observed, and the improvement on the SA is negligible. The results indicate that the two proposed controllers can improve the ride comfort and maintain the same level of SA for the IWM-suspension system. Note that although the SA of hybrid-ADD is worse than hybrid, the improvement in the SMA and less sensor number requirement are the advantages of the proposed hybrid-ADD. For RS, it can be seen that the

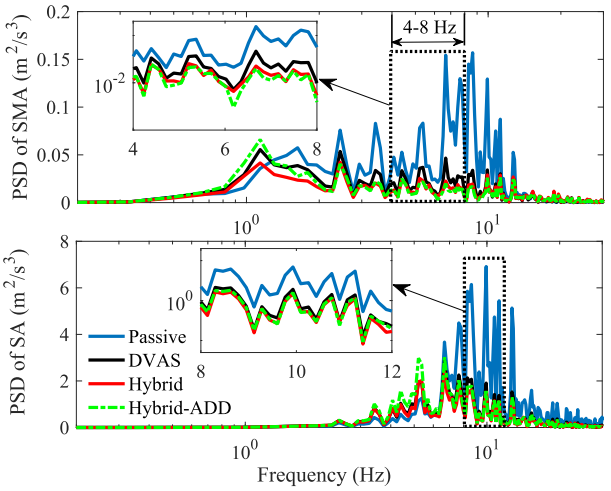

FIGURE 8. PSD comparison for random road excitation.

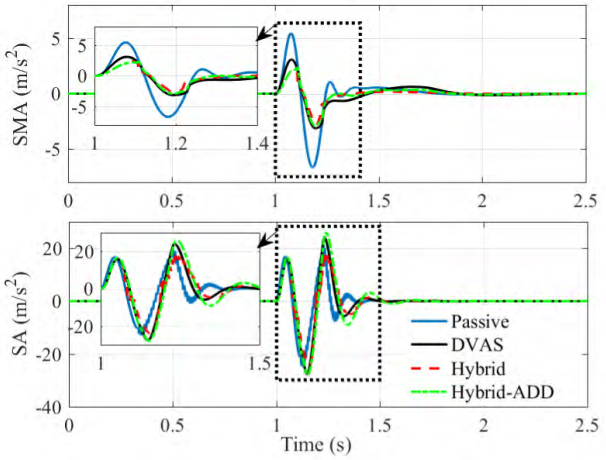

FIGURE 9. Time domain comparison for bumpy input.

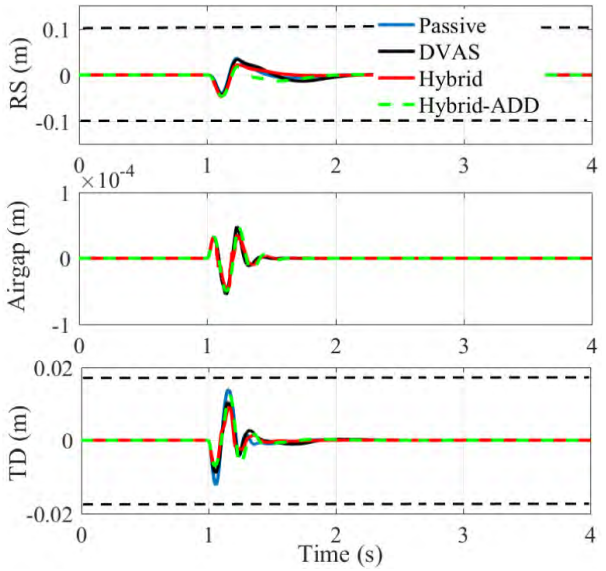

FIGURE 10. Comparison of system constraints for bumpy input.

three DVAS based systems perform worse than the passive one, which means the novel structure will deteriorate the RS response. Besides, TD comparison result shows the three structures with DVAS have a better road handling ability, and the conclusion that the DVAS structure can effectively reduce tire dynamic loading can be drawn. Of the three DVAS based IWM-suspension systems, we can see that the hybrid controller outperforms the rest on the Airgap, while the difference between the hybrid-ADD controller and the DVAS is not apparent. This result can be interpreted as the hybrid controller can reduce the vibration of the SRM better than the hybrid-ADD controller and the DVAS structure, which can also be seen from the SA comparison.

As for the PSD comparison shown in Fig. 8, it can be seen from the upper figure that all three DVAS based IWM-suspension systems can reduce SMA amplitude in the whole frequency domain. For the frequency range with which human beings are most sensitive, i.e., 4-8 Hz, both the hybrid and hybrid-ADD controllers outperform the other structures, which means better ride comfort can be expected with the proposed algorithms. In the case of the SA, the lower figure in Fig. 8 shows that all DVAS based systems can remarkably reduce vibration amplitude, and the differences of these three structures are not noticeable.

The simulation results for bumpy input are shown in Fig. 9. We can see from the SMA comparison results that the three DVAS based structures have a smaller SMA amplitude than the passive one, and both the hybrid and the hybrid-ADD controllers have the smaller convergence time. As for the SA depicted in the lower figure, the difference of all four systems is not distinct. The reason of this is that the bumpy input with the velocity v=40 km/h results in a single frequency excitation with the amplitude appearing at 6 Hz, and the PSD comparison shown in the lower figure of Fig. 8 indicates that all four systems perform similarly at this frequency.

To ensure system responses satisfy all the constraints defined in (21), system responses of RS, Airgap, and TD are shown in Fig. 10. Results show that all three responses do not violate the constraints, which means the proposed controllers settle the MOOP.

C. MBS VALIDATION

Numerical simulation results have shown the superiority of the proposed controllers over the traditional ones. Note that the simplified models defined by (13), (14) provide only the dynamic relationships of different masses, and it is of great importance to validate the feasibility of the proposed controller by fully considering the interactions between the SRM and the suspension system. In this part, this paper creates a multi-body model of the DVAS based IWM-suspension system, and then validates the proposed controllers in LMS-Motion software. Inspired by [53], the created model is shown in Fig. 11. As can be seen from this figure, a hole in the axle (11) along with a linear bearing (10)

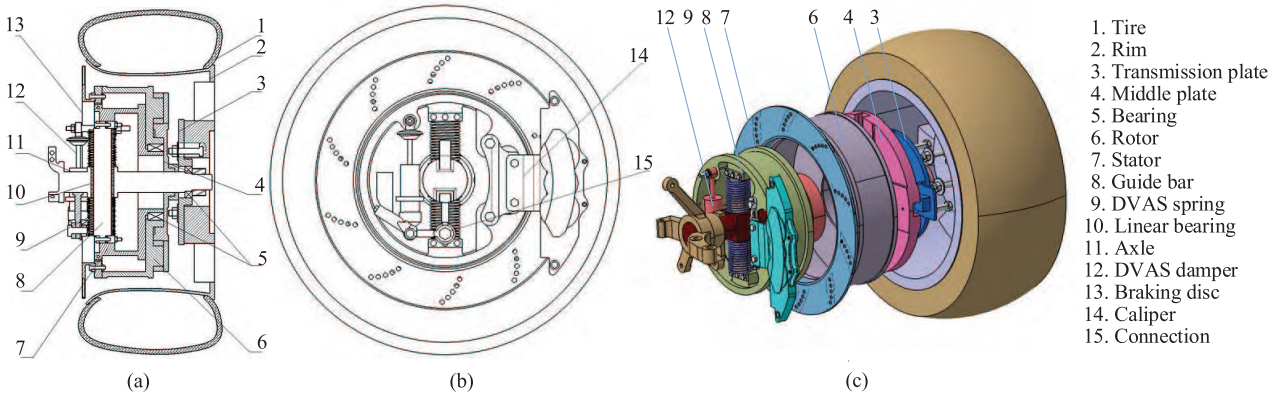

FIGURE 11. Structure of the DVAS based IWM-suspension system, (a) Side view, (b) Front view, (c) Exploded view.

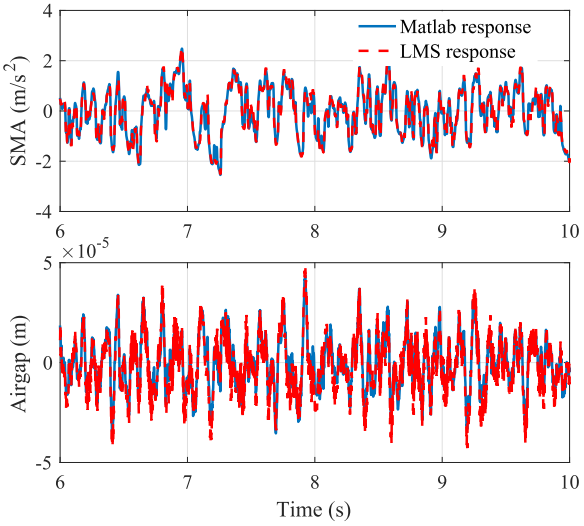

FIGURE 12. Comparison of MBS and (14).

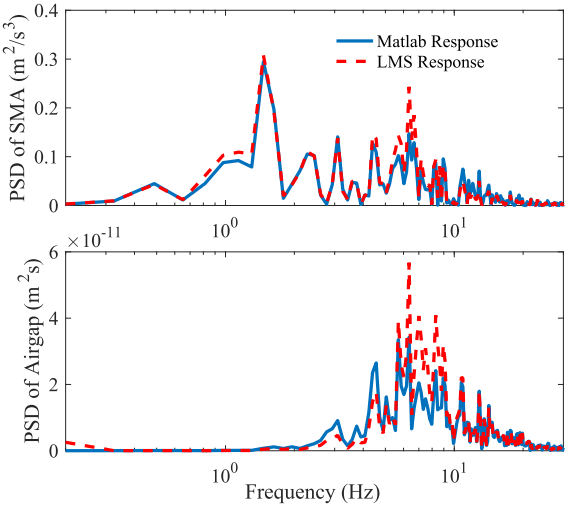

FIGURE 13. PSD comparison of MBS and (14).

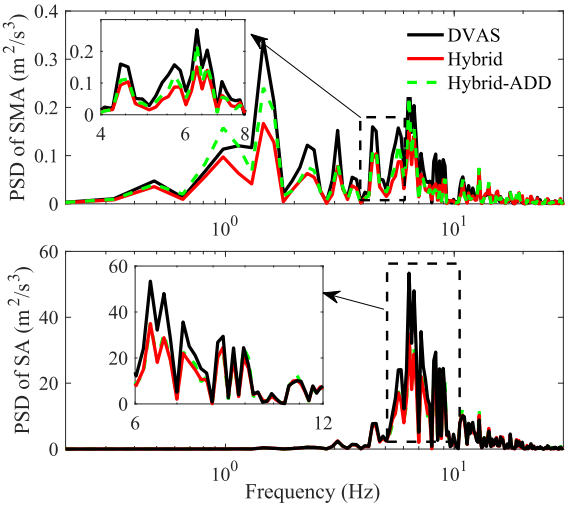

FIGURE 14. PSD comparison of different controllers in MBS.

allow vertical movement of the guide bar (8), which suspends the SRM on the axle. Both the spring (9) and the controllable damper (12) installed between the stator and the axle form the DVAS. A set of Oldham coupling, i.e., (3) and (4), is installed between the rotor (6) and the rim (2) to allow the relative vertical movement and maintain the equal angular speed for the stator and the rotor.

The model shown in (14) is first validated with the multi-body model under road excitation of ISO-C, 60 km/h, and the comparison results of SMA and airgap are given in Fig. 12 and 13. The time window length is set to be 4 s in Fig. 12 for better comparison. It can be seen from Fig. 12 that the difference between the dynamics representing by (14) and the LMS model is not apparent.

As for the PSD comparison shown in Fig. 13, we can see that the difference of the airgap around the unsprung mass resonant frequency is obvious. This phenomenon can be interpreted as the result of the unmodeled rotating components and the inertia of the rotor and connections. Since the overall trend of both the responses is the same as shown in the lower plot of Fig. 12, it introduces that the created dynamic model can accurately depict the characteristics containing in the coupled dynamics.

The PSD comparisons of different controllers in the MBS are depicted in Fig. 14. In the upper plot of Fig. 14, It can be seen that the two proposed controller outperform the DVAS, especially in the frequency range of 4-8 Hz, which stay the same with Fig. 8. As for the SA comparison, The difference of all three DVAS based structures are not apparent, indicating the proposed controllers can retain the improved stator acceleration compared to the passive structure without the DVAS.

VI. CONCLUSION

This paper presented theoretical and simulation studies for IWM driven EVs to reduce the vibration caused by unknown road disturbance and SRM induced UEMF. Based on the DVAS structure, novel yet simple hybrid control algorithms were proposed for the IWM-suspension system. Different from the previous hybrid controller used in the traditional suspension system, the proposed algorithms had multiple inputs, and two commercially available semi-active dampers were used to reproduce the virtual behavior of the dampers. A novel hybrid-ADD controller was presented, which used only half of the sensors compared to the previously proposed hybrid controller. Numerical simulation results showed that the DVAS structure can improve ride comfort and IWM vibration compared to the IWM driven EVs without the DVAS, and both the hybrid and the hybrid-ADD controllers can further improve SMA. A multi-body IWM-suspension model was finally created in LMS-Motion software, and the simulation results proved the feasibility of the novel control algorithms.

Further research will focus on the following three aspects:

- Application of advanced control strategies;
- Usage of active actuators in the novel structure;
- Experimental validation for the DVAS based IWM-suspension system.

REFERENCES

[1] Y. Huang *et al.*, "A review of power management strategies and component sizing methods for hybrid vehicles," *Renew. Sustain. Energy Rev.*, vol. 96, pp. 132–144, Nov. 2018.

[2] Y. Huang, A. Khajepour, M. Khazraee, and M. Bahrami, "A comparative study of the energy-saving controllers for automotive air-conditioning/refrigeration systems," *J. Dyn. Syst., Meas., Control*, vol. 139, no. 1, p. 014504, 2017.

[3] T. Liu, X. Hu, S. E. Li, and D. Cao, "Reinforcement learning optimized look-ahead energy management of a parallel hybrid electric vehicle," *IEEE/ASME Trans. Mechatronics*, vol. 22, no. 4, pp. 1497–1507, Aug. 2017.

[4] X. Tang, X. Hu, W. Yang, and H. Yu, "Novel torsional vibration modeling and assessment of a power-split hybrid electric vehicle equipped with a dual-mass flywheel," *IEEE Trans. Veh. Technol.*, vol. 67, no. 3, pp. 1990–2000, Mar. 2017.

[5] W. Zhao, H. Zhang, and Y. Li, "Displacement and force coupling control design for automotive active front steering system," *Mech. Syst. Signal Process.*, vol. 106, pp. 76–93, Jun. 2018.

[6] J. Zhao, "Chassis integrated control for active suspension, active front steering and direct yaw moment systems using hierarchical strategy," *Veh. Syst. Dyn.*, vol. 55, no. 1, pp. 72–103, 2017.

[7] F. Zhang, H. Liu, Y. Hu, and J. Xi, "A supervisory control algorithm of hybrid electric vehicle based on adaptive equivalent consumption minimization strategy with fuzzy pi," *Energies*, vol. 9, no. 11, p. 919, 2016.

[8] C. Hu, R. Wang, F. Yan, Y. Huang, H. Wang, and C. Wei, "Differential steering based yaw stabilization using ismc for independently actuated electric vehicles," *IEEE Trans. Intell. Transp. Syst.*, vol. 19, no. 2, pp. 627–638, Feb. 2018.

[9] J. Guo, Y. Luo, K. Li, and Y. Dai, "Coordinated path-following and direct yaw-moment control of autonomous electric vehicles with sideslip angle estimation," *Mech. Syst. Signal Process.*, vol. 105, pp. 183–199, May 2018.

[10] E. Bostanci, M. Moallem, A. Parsapour, and B. Fahimi, "Opportunities and challenges of switched reluctance motor drives for electric propulsion: A comparative study," *IEEE Trans. Transport. Electrific.*, vol. 3, no. 1, pp. 58–75, Mar. 2017.

[11] Y. Qin, C. He, X. Shao, H. Du, C. Xiang, and M. Dong, "Vibration mitigation for in-wheel switched reluctance motor driven electric vehicle with dynamic vibration absorbing structures," *J. Sound Vib.*, vol. 419, pp. 249–267, Apr. 2018.

[12] M. Takiguchi, H. Sugimoto, N. Kurihara, and A. Chiba, "Acoustic noise and vibration reduction of SRM by elimination of third harmonic component in sum of radial forces," *IEEE Trans. Energy Convers.*, vol. 30, no. 3, pp. 883–891, Sep. 2015.

[13] W. Sun, Y. Li, J. Huang, and N. Zhang, "Vibration effect and control of in-wheel switched reluctance motor for electric vehicle," *J. Sound Vib.*, vol. 338, pp. 105–120, Mar. 2015.

[14] B. Hredzak, S. Gair, and J. F. Eastham, "Control of an EV drive with reduced unsprung mass," *IEE Proc.–Electr. Power Appl.*, vol. 145, no. 6, pp. 600–606, Nov. 1998.

[15] G. Nagaya, Y. Wakao, and A. Abe, "Development of an in-wheel drive with advanced dynamic-damper mechanism," *JSAE Rev.*, vol. 24, no. 4, pp. 477–481, 2003.

[16] D. Cao, X. Song, and M. Ahmadian, "Editors' perspectives: Road vehicle suspension design, dynamics, and control," *Vehicle Syst. Dyn.*, vol. 49, nos. 1–2, pp. 3–28, 2011.

[17] W. Sun, H. Pan, and H. Gao, "Filter-based adaptive vibration control for active vehicle suspensions with electrohydraulic actuators," *IEEE Trans. Veh. Technol.*, vol. 65, no. 6, pp. 4619–4626, May 2016.

[18] J. Zhao, P. K. Wong, X. Ma, and Z. Xie, "Design and analysis of an integrated sliding mode control–two-point wheelbase preview strategy for a semi-active air suspension with stepper motor-driven gas-filled adjustable shock absorber," *Proc. Inst. Mech. Eng. I, J. Syst. Control Eng.* vol. 232, no. 9, pp. 1194–1211.

[19] H. Pan, X. Jing, and W. Sun, "Robust finite-time tracking control for nonlinear suspension systems via disturbance compensation," *Mech. Syst. Signal Process.*, vol. 88, pp. 49–61, May 2017.

[20] H. Pan, X. Jing, W. Sun, and H. Gao, "A bioinspired dynamics-based adaptive tracking control for nonlinear suspension systems," *IEEE Trans. Control Syst. Technol.*, vol. 26, no. 3, pp. 903–914, May 2017.

[21] X. Tang, H. Du, S. Sun, D. Ning, Z. Xing, and W. Li, "Takagi–Sugeno fuzzy control for semi-active vehicle suspension with a magnetorheological damper and experimental validation," *IEEE/ASME Trans. Mechatronics*, vol. 22, no. 1, pp. 291–300, Feb. 2017.

[22] X. Shao, F. Naghdy, and H. Du, "Reliable fuzzy H∞ control for active suspension of in-wheel motor driven electric vehicles with dynamic damping," *Mech. Syst. Signal Process.*, vol. 87, pp. 365–383, Mar. 2017.

[23] R. Wang, H. Jing, F. Yan, H. R. Karimi, and N. Chen, "Optimization and finite-frequency H∞ control of active suspensions in in-wheel motor driven electric ground vehicles," *J. Franklin Inst.*, vol. 352, no. 2, pp. 468–484, 2015.

[24] D. Tan and C. Lu, "The influence of the magnetic force generated by the in-wheel motor on the vertical and lateral coupling dynamics of electric vehicles," *IEEE Trans. Veh. Technol.*, vol. 65, no. 6, pp. 4655–4668, Jun. 2016.

[25] X. Xue *et al.*, "Optimal control method of motoring operation for SRM drives in electric vehicles," *IEEE Trans. Veh. Technol.*, vol. 59, no. 3, pp. 1191–1204, Mar. 2010.

[26] A. Khalil and I. Husain, "A Fourier series generalized geometry-based analytical model of switched reluctance machines," *IEEE Trans. Ind. Appl.*, vol. 43, no. 3, pp. 673–684, May 2007.

[27] R. Krishnan, *Switched Reluctance Motor Drives: Modeling, Simulation, Analysis, Design, and Applications*. Boca Raton, FL, USA: CRC Press, 2001.

[28] R. Rajamani, *Vehicle Dynamics and Control*. New York, NY, USA: Springer, 2011.

[29] Y. Qin, Z. Wang, C. Xiang, M. Dong, C. Hu, and R. Wang, "A novel global sensitivity analysis on the observation accuracy of the coupled vehicle model," *Vehicle Syst. Dyn.*, 2019. [Online]. Available: https://www.tandfonline.com/doi/abs/10.1080/00423114.2018.1517219, doi: 10.1080/00423114.2018.1517219.

[30] Z. Wang, M. Dong, L. Gu, J. Rath, Y. Qin, and B. Bai, "Influence of road excitation and steering wheel input on vehicle system dynamic responses," *Appl. Sci.*, vol. 7, no. 6, p. 570, 2017.
[31] Z. Wang, Y. Qin, L. Gu, and M. Dong, "Vehicle system state estimation based on adaptive unscented Kalman filtering combing with road classification," *IEEE Access*, vol. 5, pp. 27786–27799, 2017.
[32] J. J. Rath, K. C. Veluvolu, and M. Defoort, "Simultaneous estimation of road profile and tire road friction for automotive vehicle," *IEEE Trans. Veh. Technol.*, vol. 64, no. 10, pp. 4461–4471, Oct. 2015.
[33] Y. Qin, F. Zhao, Z. Wang, L. Gu, and M. Dong, "Comprehensive analysis for influence of controllable damper time delay on semi-active suspension control strategies," *J. Vib. Acoust.*, vol. 139, no. 3, p. 031006, 2017.
[34] S. Sun *et al.*, "A compact variable stiffness and damping shock absorber for vehicle suspension," *IEEE/ASME Trans. Mechatronics*, vol. 20, no. 5, pp. 2621–2629, Oct. 2015.
[35] B. F. Spencer, Jr., S. J. Dyke, M. K. Sain, and J. D. Carlson, "Phenomenological model for magnetorheological dampers," *ASCE J. Eng. Mech.*, vol. 123, no. 3, pp. 230–238, Mar. 1997.
[36] X. M. Dong, M. Yu, C. R. Liao, and W. M. Chen, "Comparative research on semi-active control strategies for magneto-rheological suspension," *Nonliear Dyn.*, vol. 59, no. 3, pp. 433–453, Feb. 2010.
[37] X. Zhang, Z. Li, K. Guo, F. Zheng, and Z. Wang, "A novel pumping magnetorheological damper: Design, optimization, and evaluation," *J. Intell. Mater. Syst. Struct.*, vol. 28, no. 17, pp. 2339–2348, 2017.
[38] X. Song, M. Ahmadian, and S. C. Southward, "Modeling magnetorheological dampers with application of nonparametric approach," *J. Intell. Mater. Syst. Struct.*, vol. 16, no. 5, pp. 421–432, 2005.
[39] Y. Qin, M. Dong, R. Langari, L. Gu, and J. Guan, "Adaptive hybrid control of vehicle semiactive suspension based on road profile estimation," *Shock Vib.*, vol. 2015, Apr. 2015, Art. no. 636739.
[40] J. J. Rath, M. Defoort, H. R. Karimi, and K. C. Veluvolu, "Output feedback active suspension control with higher order terminal sliding mode," *IEEE Trans. Ind. Electron.*, vol. 64, no. 2, pp. 1392–1403, Feb. 2017.
[41] K. N. Srinivas and R. Arumugam, "Static and dynamic vibration analyses of switched reluctance motors including bearings, housing, rotor dynamics, and applied loads," *IEEE Trans. Magn.*, vol. 40, no. 4, pp. 1911–1919, Jul. 2004.
[42] D. Karnopp, M. J. Crosby, and R. A. Harwood, "Vibration control using semi-active force generators," *Int. J. Eng. Ind.*, vol. 96, no. 2, pp. 619–626, 1974.
[43] M. Ahmadian and C. A. Pare, "A quarter-car experimental analysis of alternative semiactive control methods," *J. Intell. Mater. Syst. Struct.*, vol. 11, no. 8, pp. 604–612, 2000.
[44] S. M. Savaresi, E. Silani, S. Bittanti, and N. Porciani, "On performance evaluation methods and control strategies for semi-active suspension systems," in *Proc. 42nd IEEE Conf. Decis. Control*, vol. 3, Dec. 2003, pp. 2264–2269.
[45] M. Gobbi and G. Mastinu, "Analytical description and optimization of the dynamic behaviour of passively suspended road vehicles," *J. Sound Vib.*, vol. 245, no. 3, pp. 457–481, 2001.
[46] Q. Zhang and H. Li, "MOEA/D: A multiobjective evolutionary algorithm based on decomposition," *IEEE Trans. Evol. Comput.*, vol. 11, no. 6, pp. 712–731, Dec. 2007.
[47] M. A. Jan and Q. Zhang, "MOEA/D for constrained multiobjective optimization: Some preliminary experimental results," in *Proc. UK Workshop Comput. Intell. (UKCI)*, 2010, pp. 1–6.
[48] D. Kalyanmoy, *Multi Objective Optimization Using Evolutionary Algorithms*. Hoboken, NJ, USA: Wiley, 2001.
[49] Y. Qin, C. Wei, X. Tang, N. Zhang, M. Dong, and C. Hu, "A novel nonlinear road profile classification approach for controllable suspension system: Simulation and experimental validation," *Mech. Syst. Signal Process.* Oct. 2018. [Online]. Available: https://www.sciencedirect.com/science/article/pii/S0888327018304163, doi: 10.1016/j.ymssp.2018.07.015.
[50] Y. Qin, C. Xiang, Z. Wang, and M. Dong, "Road excitation classification for semi-active suspension system based on system response," *J. Vib. Control*, vol. 24, no. 13, pp. 2732–2748, 2018.
[51] Y. Qin, Z. Wang, C. Xiang, E. Hashemi, A. Khajepour, and Y. Huang, "Speed independent road classification strategy based on vehicle response: Theory and experimental validation," *Mech. Syst. Signal Process.*, vol. 117, no. 2, pp. 653–666, 2019.
[52] F. Zhao, S. S. Ge, F. Tu, Y. Qin, and M. Dong, "Adaptive neural network control for active suspension system with actuator saturation," *IET Control Theory Appl.*, vol. 10, no. 14, pp. 1696–1705, 2016.
[53] Y. Ma, Z. Deng, and D. Xie, "Control of the active suspension for in-wheel motor," *J. Adv. Mech. Des. Syst. Manuf.*, vol. 7, no. 4, pp. 535–543, 2013.

BIN XU received the B.Sc. and Ph.D. degrees in mechanical engineering from the Beijing Institute of Technology, China, in 2005 and 2013, respectively. From 2016 to 2017, he was with the University of California at Berkeley, Berkeley, as a Visiting Scholar. He is currently an Associate Professor with the Vehicle Research Center, Beijing Institute of Technology. His research interests include aerial and ground vehicle, and its dynamic control.

CHANGLE XIANG received the B.E., M.E., and Ph.D. degrees from the Beijing Institute of Technology, China, in 1984, 1987, and 2001 respectively. From 1999 to 2000, he was a Senior Visiting Scholar with Wayne State University. He is currently a Professor of mechanical engineering with the Beijing Institute of Technology. He has published over 150 peer reviewed papers. His research interests include vehicle transmission theory and vehicle system dynamics.

YECHEN QIN (SM'12–M'16) received the B.Sc. and Ph.D. degrees in mechanical engineering from the Beijing Institute of Technology, China, in 2010 and 2016, respectively. He is currently pursuing the Ph.D. degree with the Beijing Institute of Technology. From 2013 to 2014, he was with in Texas A&M University, USA, as a visiting Ph.D. student. From 2017 to 2018, he was with the University of Waterloo as a Visiting Scholar. His research interests include controllable suspension systems, in wheel motor vibration control, and intelligent vehicle dynamics control.

PENG DING received the bachelor's degree in mechanical engineering from the China University of Geosciences, Beijing, in 2017. He is currently pursuing the master's degree with the Beijing Institute of Technology. His research interests include suspension systems and vibration control of wheel hub motors.

MINGMING DONG received the Ph.D. degree from the Beijing Institute of Technology in 2003. From 2017 to 2018, he was with the University of Wollongong as a Visiting Scholar. He is currently the Director of the Noise and Vibration Laboratory, Beijing Institute of Technology. His research areas include suspension system dynamics, in wheel motor vibration control, modeling and estimation, and modeling for lightweight vehicles suspension systems.